Published in final edited form as:
RSC Adv. 2015 January 1; 5(4): 2411–2420. doi:10.1039/c4ra10871j.

Nanodelivery of Parthenolide Using Functionalized Nanographene Enhances its Anticancer Activity

A. Karmakar[a], **Y. Xu**[a], **T. Mustafa**[a,†], **G. Kannarpady**[a], **S.M. Bratton**[b], **A. Radominska-Pandya**[b], **P.A. Crooks**[b], and **A.S. Biris**[a]

Y. Xu: yxxu@ualr.edu; A.S. Biris: asbiris@ualr.edu

[a]Center for Integrative Nanotechnology Sciences, University of Arkansas at Little Rock, AR 72204, USA

[b]Department of Biochemistry and Molecular Biology, College of Medicine, University of Arkansas for Medical Sciences, Little Rock, AR, 72205, USA

[c]Department of Pharmaceutical Sciences, College of Pharmacy, University of Arkansas for Medical Sciences, Little Rock, AR 72205, USA

Abstract

Advances in anticancer chemotherapy have been hindered by the lack of biocompatibility of new prospective drugs. One significant challenge concerns water insolubility, which compromises the bioavailability of the drugs leading to increased dosage and higher systemic toxicity. To overcome these problems, nanodelivery has been established as a promising approach for increasing the efficacy and lowering the required dosage of chemotherapeutics. The naturally derived compound, parthenolide (PTL), is known for its anti-inflammatory and anticancer activity, but its poor water solubility limits its clinical value. In the present study, we have used carboxyl-functionalized nanographene (fGn) delivery to overcome the extreme hydrophobicity of this drug. A water-soluble PTL analog, dimethylamino parthenolide (DMAPT), was also examined for comparison with the anticancer efficacy of our PTL-fGn complex. Delivery by fGn was found to increase the anticancer/apoptotic effects of PTL (but not DMAPT) when delivered to the human pancreatic cancer cell line, Panc-1. The IC_{50} value for PTL decreased from 39 μM to 9.5 μM when delivered as a mixture with fGn. The IC_{50} of DMAPT did not decrease when delivered as DMAPT-fGn and was significantly higher than that for PTL-fGn. There were significant increases in ROS formation and in mitochondrial membrane disruption in Panc-1 cells after PTL-fGn treatment as compared to PTL treatment, alone. Increases in toxicity were also seen with apoptosis detection assays using flow cytometry, ethidium bromide/acridine orange/DAPI staining, and TUNEL. Thus, fGn delivery was successfully used to overcome the poor water solubility of PTL, providing a strategy for improving the effectiveness of this anticancer agent.

Correspondence to: Y. Xu, yxxu@ualr.edu; A.S. Biris, asbiris@ualr.edu.

†Currently with the Department for Biology, College of Sciences for Women, University of Baghdad, Bagdhad, Iraq.

The authors disclose no potential conflict of interest.

Electronic Supplementary Information (ESI) available:. See DOI: 10.1039/b000000x/

Introduction

Pancreatic cancer is the fourth leading cause of cancer-related death in the USA making it one of the most deadly forms of cancer in humans. Despite recent advancements in modern cancer detection and treatment, the mortality rate of this cancer is almost identical to the occurrence, with a 5-year survival rate of only 6%.[1] Pancreatic cancer is known to be extremely resistant to many widely used anti-cancer drugs, which makes it insensitive to conventional chemotherapy.[2] The most common way of administering chemotherapeutic drugs is through the systemic pathway; as a result, drug molecules have to pass through the vasculature and the interstitial space of the tumor before reaching tumor cells.[3] These pathways are affected by a number of factors: diffusion of the drug molecule, interaction of the drug molecule with various intra- and extra-cellular moieties, solid tumor environment, interstitial pressure, angiogenesis of the tumor vasculature, tumor cell density, and tumor blood flow.[4] Delivery of an effective dose of drug to solid tumors becomes extremely challenging, due to the presence of these multiple barriers. The most successful approach is a combination of multiple classes of anti-cancer agents, but even this is only able to increase the one-year survival rate to 35%.[5] Thus, the search for novel and efficacious agents to treat pancreatic cancer continues.

Parthenolide (PTL) is a sesquiterpene lactone extracted from *Tanacetumparthenium*, commonly known as feverfew. The reactive α-methylene-γ-lactone moiety and epoxide ring of PTL are capable of reacting with nucleophilic moieties on bio-molecules.[6] Although PTL has long been used as a medication for migraine headache and rheumatoid arthritis, primarily due to its anti-inflammatory activity,[7] recently, this drug has been investigated for the treatment of several cancers, including pancreatic cancer.[8] Along with its anti-proliferative and apoptotic activity in different cancer cell lines *in vitro*, PTL also sensitizes cancer cells to other anticancer agents[9–11] and has been identified as a radio sensitization agent. PTL has been shown to induce apoptosis through multiple pathways, including oxidative stress due to ROS generation,[12] mitochondrial membrane potential disruption,[13] caspase activation,[12,13] and NF-κB inhibition.[14–17] Recently, we have shown that PTL can selectively induce almost complete glutathione depletion and severe cell death in cancerous CD34+ acute myeloid leukemia cells.[18] Interestingly, PTL induces significantly less toxicity and only limited, transient glutathione depletion in normal CD34+ cells. This specificity of action in cancer cells greatly increases the appeal of this potential anti-cancer therapy; however, the usefulness of this drug is been hampered by its poor solubility, which leads to limited bioavailability. In an attempt to overcome this problem, the water-soluble PTL analog, dimethylamino parthenolide (DMAPT), was developed to improve oral bioavailability.[19–21] This PTL-derivative has been shown to be effective against acute myeloid leukemia[19] in phase 1 clinical trials.

Nonetheless, there is still benefit to be gained by finding additional ways to increase the solubility and efficacy of PTL and to increase its intracellular concentrations to effective dosage levels. Nanotechnology represents an excellent option for solving these problems because of the unique chemical, physical, and mechanical properties of nanomaterials. We have shown that nanoparticles have great potential for use in the biomedical field, e.g., disease detection,[22] hyperthermia,[23] gene delivery,[24] and drug delivery.[25] In fact, several

types of nanoparticles have been used as drug carriers, including carbon nanotubes, magnetic nanoparticles, mesoporous nanomaterials, gold nanoparticles, etc.[26]

Recently, graphene (Gn), a two-dimensional, sp^2 hybridized carbon nanomaterial with one atomic layer, has generated considerable interest in the field of materials science;[27–33] however, its use in the biomedical field is still in the early stages of development.[34] Due to its distinctive structural features—high specific surface area and large sp2-bonded carbon atomic plane—Gn provides an optimum platform for drug loading and delivery. For example, the π-π stacking ability of Gn is a desirable characteristic for most drug loading applications.[34] In addition, the surface of Gn can be chemically modified and customized through relatively facile procedures to make it an even more customable drug-delivery tool. Gn-oxide, with oxygen-rich functional groups on its surface, demonstrates extraordinary biocompatibility, stability, and solubility at physiological conditions. Furthermore, targeting biomolecules can also be added to direct the drug-particle complexes specifically to cancer cells, which would lead to an increase in the delivery of drugs to cancer cells.

In the current study, we demonstrate the ability of *carboxyl*-functionalized graphene (fGn) to enhance the delivery of the anticancer drug PTL to the pancreatic cancer cell line, Panc-1. Apoptotic and anticancer activities were determined by measuring ROS generation, mitochondrial health and membrane integrity, caspase activity, cell membrane permeability, and DNA fragmentation. The PTL-fGn formulation demonstrated a significant improvement in the anticancer/apoptotic effects *in vitro* as compared PTL, alone. Thus, the nanodelivery of PTL by fGn, described here for the first time, improves the overall efficacy of PTL in Panc-1 cells, highlighting the potential of this approach to improving the therapeutic effectiveness of this promising anticancer agent.

Experimental Section

Synthesis and characterization of nanomaterials

Carboxyl-functionalized Graphene (fGn)—Gn was purchased from Angstron Materials Inc. (Dayton, OH, USA). Gn (10 mg) was added to a mixture of H_2SO_4 and HNO_3. The mixture was sonicated for 4–5 h and then filtered through a 0.2 μm GTTP membrane (Millipore, USA) and washed with deionized water several times. The resulting fGn powder was oven-dried overnight at 100°C and then placed in a vacuum dessicator. For use in subsequent experiments, the fGn powder was re-dispersed in deionized water by sonication.

Characterization of Gn and fGn—TEM images were collected on a field emission JEM-2100F transmission electron microscopy (JEOL Inc.) equipped with CCD camera. The acceleration voltage was 100 kV for the Gn and fGn analysis. Gn and fGn powder was highly dispersed in the ethanol solution with 30 min of sonication. A few drops of suspension were deposited on the TEM grid to dry before the analysis. Gn or fGn powders were dispersed into deionized water with sonication about 1 hour to form 50 μg/ml stock solutions. Certain dilutions were needed to perform the Zeta potential analysis (ZETA-READER MARK 21, Zeta potential Instruments, Inc., Bedminster, NJ).

Loading of PTL and DMAPT onto fGn—PTL was obtained from Sigma-Aldrich (USA). DMAPT was synthesized from PTL as previously reported[35] and was used as the fumarate salt. PTL and DMAPT were dissolved in DMSO to create 10 mM stock solutions. To create the PTL-fGn and DMAPT-fGn complexes, the drug was added to fGn solution in media (final drug-fGn complex concentrations were 1, 10, 20, 30, 50, and 100 μM drug and 10 μg/ml fGn), sonicated for 1 h, and then stored at 4°C before being incubated with Panc-1 cells. The chemical structures of Parthenolide and DMAPT are given in Figure 1.

X-ray Photoelectron Spectroscopy (XPS) analysis of the PTL–fGn interactions —XPS analysis was used to investigate the interactions between fGN and PTL. The data were collected using a K-Alpha X-ray Photoelectron Spectrometer (XPS) system at a background pressure of 1×10^{-9} torr, using a monochromated Al Kα ($h\upsilon$ = 1436.6 eV) x-ray source. The x-ray beam used was 36W, 400 μm in diameter. Survey scans (0 – 1350 eV) were taken of each sample at a pass energy (CAE) of 200 eV and 1 eV step size. The collected data were referenced to the C1s' peak to 284.5 eV based on the data obtained for adventitious carbon grown on a glass slide. Narrow scans (25 – 40 eV width) of the peaks of interest (C1s) were taken at pass energy of 50 eV and 0.1 eV step size to provide higher resolution analysis of the peaks. Curve fitting was performed using Shirley, Powell, and simplex models on the narrow scans using the Avantage V. 5.38 software.

Cell culture conditions

The human pancreatic cancer cell line, Panc-1, was purchased from the American Type Culture Collection (ATCC; USA). Cells were cultured in in T-75 culture flasks with Dulbecco's Modified Eagle Medium (DMEM; Gibco, Life Technologies, USA) containing 10% fetal bovine serum and 1% penicillin-streptomycin solution in a humidified incubator at 37°C and 5% CO_2. The medium was changed every 2 to 3 days, and the cells were sub-cultured when they reached ~90% confluence.

Analysis of fGn internalization in Panc-1 cells using Transmission Electron Microscopy (TEM)

To visualize the internalization of fGn in Panc-1 cells, transmission electron microscopy (TEM) was performed on sections of Panc-1 cells after treatment with to fGn. After incubation, Panc-1 cells were fixed with 3% glutaraldehyde in 0.1 M phosphate buffer, pH 7.2, overnight at 4°C. Following fixation, the cells were vigorously rinsed with 0.1 M phosphate buffer (pH 7.2), and put through a second fixation with 2% OsO_4 in 0.1 M phosphate buffer for 2 h and rinsed with deionized water, followed by a final dehydration step in ethanol solution.

The dehydrated and fixed cells were then embedded in polymerized epoxy resin, and an ultra microtome, Model EM UC7 (Leica microsystems GmbH, Wetzlar, Germany), was used to obtain sections with thicknesses of 0.5–1.0 μm and 60–100 nm. After staining with heavy metal (uranyl acetate and lead citrate), the 60–100 nm sections were mounted on 100 mesh formvar-carbon coated copper grids, and covered with a thin layer of carbon and analyzed under a JEM-2100F Transmission Electron Microscope (TEM) (JEOL, Peabody, Massachusetts, USA) with an accelerating voltage of 80kV.

Estimating cell viability by measuring mitochondrial dehydrogenase activity— Determination of concentration- and time-dependent cytotoxicity was carried out using the WST-1 assay (Roche Applied Science, USA). Panc-1 cells were seeded in 96-well plates for 24 hours, after which the cells were treated with nanomaterial and/or drug. After incubation, the treatment medium was removed, and the cells were washed 3 times with 1× PBS buffer. 100 μl of fresh complete growth medium were then added to each well, followed by 10 μl of the WST-1 reagent. The plates were then incubated in the dark at 37°C. After 2 h, absorbance was measured using an iMark microplate (Bio-Rad, USA) reader at a wavelength of 450 nm. All of the control and treatment samples were run in triplicate.

Cytotoxicity of Gn and fGn in Panc-1 cells—In order to compare the cytotoxicity of Gn to that of fGn and to select a "non-toxic" concentration for fGn to use in future nanodelivery experiments, cells (15,000 seeded per well) were treated with increasing concentrations (5, 10, 20, and 50 μg/ml) of Gn and fGn, for 24 h, and metabolic activity was measured as described above.

Cytotoxicity of PTL, DMAPT, PTL-fGn and DMAPT-fGn in Panc-1 cells—In order to compare the cytotoxicity of PTL and DMAPT to that of PTL-fGn and DMAPT-fGn, cells were treated with increasing concentrations (0, 1, 10, 20, 50, and 100 μM) of PTL and DMAPT and corresponding concentrations of these to compounds loaded onto fGn (10 μg/ml). Cells (10,000 seeded per well) were incubated for 24 h, and metabolic activity was measured as described above. PTL was delivered in DMSO and final incubations contained ≤1% DMSO.

Quantitation of reactive oxygen species (ROS) levels

ROS levels were determined using 2',7'-dichlorofluorescein diacetate dye (DCFH-DA; Sigma-Aldrich, USA). Briefly, Panc-1 cells were seeded (25,000 per well) in 96-well plates for 24 hours. Cells were then incubated with increasing concentrations of PTL (either alone or delivered by 10 mg/ml fGn) for 24 h. Cells were then washed with 1× PBS. DMEM medium (without FBS or antibiotics) containing 20 μM of DCFH-DA dye was added to each well, and the plate was incubated in the dark at 37°C for 30 minutes. After incubation, the fluorescence of each well was determined using a Hybrid Multi-Mode Microplate Reader (Synergy H1, BioTek, USA) at an excitation wavelength of 480 nm and an emission wavelength of 528 nm. Data were analyzed using two-way ANOVA (Bonferroni post-test).

Mitochondrial membrane polarity determination

JC-1 (5',6,6'-tetrachloro-1,1',3,3'- tetraethylbenzimidazolylcarbocyanine iodide) dye (Life Technologies, USA) was used to evaluate the mitochondrial membrane potential ($\Delta\Psi_m$) and integrity of treated Panc-1 cells. Cells were seeded in an 8-chambered slide (50,000 cells per chamber) and allowed to attach for 24 hours. Cell attachment was followed by drug or control treatments, and slides were incubated for 24 hours. The medium was then removed carefully, and complete DMEM medium containing 10 μg/ml of JC-1 dye was added to each well. The slides were then incubated for 30 min. in the dark at 37°C. Next, cells were washed with 1× PBS, and fluorescence images were taken using an Olympus TRITC (red)

filter to visualize the J-aggregate in intact mitochondria and a FITC (green) filter to visualize the monomeric form in the cytoplasm, in the case of lost mitochondrial membrane polarity.

Detection of Apoptosis after PTL and PTL-fGn treatment

Caspase activity detection—To determine whether PTL-Gn treatment led to cell death via apoptosis, the levels of active caspase in treated Panc-1 cells were stained with carboxyfluorescein (FAM) labeled-peptide-fluoromethyl ketone (FMK) caspase inhibitor (FAM-Peptide-FMK) and assessed by either relative fluorescence or imaged using Fluorescence microscopy. For relative fluorescence experiments, 25,000 Panc-1 cells were seeded in each well of a black-sided, clear-bottomed, 96-well plate for 24 hours at 37°C before drug or vehicle treatment. For imaging purposes, 50,000 cells were plated in each chamber of an 8-chambered slide. Cells were then incubated with PTL (14 μM), fGn (10 μg/ml), or PTL-fGn (14 μM - 10 μg/ml) in 200 or 400 μl of medium for each well, respectively, for 24 hours at 37°C. Cells without any drug treatment served as the negative control, and 100 μM etoposide were used as a positive control. Caspase activity was then measured using the APO LOGIX Carboxyfluorescein Caspase Detection Kit (Cell Technology Inc. USA) according to manufacturer's instructions. Briefly, the necessary volume of (FAM-Peptide-FMK) solution was added to each well/chamber, and the plates were incubated in the dark for 45 min at 37°C. The cells were then washed twice with 100 μl of wash buffer (supplied with the assay kit). 100 μl of wash buffer were then added, and fluorescence was either measured using a Synergy H1 fluorescence microplate reader at an excitation wavelength of 485 nm and at an emission wavelength of 528 nm or imaged using an Olympus fluorescence microscope equipped with a FITC filter. Data were analyzed using two-way ANOVA (Bonferroni post-test).

Acridine Orange (AO)/Ethidium Bromide (EB) staining—Apoptosis was also assessed using AO/EB staining. 150,000 Panc-1 cells were seeded in each well of a 12-well plate. After 24 hours, drug and vehicle treatments were carried out. After treatment, cells were collected and pelleted by centrifugation at 1,100 rpm. Cell pellets were then re-suspended in 15 μl of fresh growth medium and 2 μl of EB/AO dye mixture (0.50 mg/ml of EB and 0.15 mg/ml of AO in 1× PBS). The mixture was then incubated at room temperature for a few minutes. The stained cells were placed on a slide, mounted with a cover slide, and immediately visualized using an Olympus fluorescence microscope with a 10× objective. Representative images were captured from random fields of view using filters appropriate for the specific fluorescent dyes and combined using the software Cell Sens Dimension software (Olympus, USA).

Terminal deoxynucleotidyl transferased UTPNick End Labeling (TUNEL)—Apoptotic activity was further investigated by TUNEL, which measures DNA fragmentation in apoptotic nuclei after PTL treatment. 100,000 Panc-1 cells were seeded in each well of a four-chambered glass slide and incubated for 24 hours at 37°C before treatment. DNA fragmentation was then measured using the QIA33 FragEL™ DNA Fragmentation Detection Kit, Colorimetric-terminal deoxynucleotidyl transferase (TdT) Enzyme; Calbiochem, USA) according to the manufacturer's instructions. Briefly, cells were fixed, rehydrated, and permeabilized using Proteinase K. Then endogenous peroxidase was

inactivated, followed by equilibration and labeling of the fragmented DNA with biotin-labeled and unlabeled deoxynucleotides using TdT. Fragmented DNA was then detected by staining with Diaminobenzidine (DAB) solution, followed by immediate counterstaining of live cells with methyl green. The samples were then mounted with mounting medium, covered with coverslips, and sealed. Images were then collected using phase contrast microscopy (Olympus BX51 Microscope).

Flow cytometry analysis after Annexin V &propidium iodide staining—A flow cytometric assay, using fluorescein isothiocyanate (FITC)-labelled Annexin V (green fluorescence) and propidium iodide (PI; red flourescence), was performed to determine the percentage of apoptotic cells in treated and non-treated groups.[36] Panc-1 cells were seeded in 12-well plates (150,000 cells per well) and allowed to attach overnight. Cells were then treated with fGn (10 μg/ml), PTL (14 μM), and PTL-fGN (14 μM - 10 μg/ml) and incubated for 48 h at 37°C. A negative control group with medium only was also included. After incubation, the assay was carried out according to the manufacturer's (BioVision, Inc.) protocol. Briefly, treated Panc-1 cells were trypsinized and centrifuged at 1100 rpm. Cell pellets were re-suspended in 500 μl of 1× binding buffer, and 5 μl each of annexin V-FITC and PI were added, followed by 5 minutes of incubation on ice. Each sample was analyzed using a FACSC alibur flow cytometer (Becton Dickinson), and Cell Quest software was used to analyze the data collected and to generate the cytogram. Differences in percentages of stained cells between treatment conditions were assessed by one-way ANOVA followed by a nonparametric Newman–Keuls multiple comparisons posttest using Graphpad Prism4 software. Results at $P<0.05$ were considered statistically significant.

Results and discussion

Analysis of Nanomaterials

Characterization of Gn an fGn—Gn used in this study was found to have 1–3 layers and is <10 μm (x–y dimension) in size which can be observed from the TEM image (Figure 2a). The Gn used in this study was further functionalized with carboxylic acid groups to form fGn. After sonication and functionalization, the size of the graphene decreased to <300–500 nm (x–y dimension; Figure 2b). The surface functionalities enhance the stability and solubility of the graphene sheets by generating negative charges on the surface with a zeta potential of -47.6 mV.

Characterization drug-fGn complexes—In the current study, we loaded PTL onto the surface of fGn through hydrophobic interactions. To determine the amount of PTL and DMAPT bound to fGn, UV-Vis spectra of drug-free fGn and PTL-fGn were recorded (Supplementary Figure 1). The successful attachment of PTL onto the fGn surface was evidenced by the characteristic absorbance peak measured at 207 nm, and the concentration of PTL was determined based on the intensity of this UV absorption band. A loading efficiency of 98.7% was calculated, indicating that almost all of the PTL drug molecules were attached to the surface of fGn. It is proposed that the hydrophobic structure of PTL causes it to interact with the carbon surface of the nanomaterial and that the carboxylate groups of fGn allow the PTL-fGn complexes to disperse readily in water.

XPS analysis of the PTL–fGn interactions—In order to study the interactions between the nanomaterial and the drug, XPS measurements of were taken of fGn, PTL, and the PTL-fGn complex (Figure 3). XPS data for C1 peaks in the fGn show characteristic peaks including the important π-π shake up peak at 290.5 eV. After the binding of PTL, this π-π shake up peak is not seen. These data support the idea that the drug binds to the nanomaterial via physical absorption (π-π stacking) as reported.[34] No other remarkable changes were seen in the spectra of fGn in the presence of PTL. This could be due to the relatively low concentration of PTL as compared to fGn in the complex.

Analysis of fGn internalization in Panc-1 cells using TEM

Prior to using fGn for our detailed drug-delivery studies, we had to determine if fGn could be easily taken up by Panc-1 cells. Therefore, Panc-1 cells were incubated with fGn (10 μg/ml) for 24 h, and cellular TEM micrographs were obtained (Figure 4). Based on observation of the TEM micrographs, the fGn sheets first adhered to the cellular membrane and were then internalized and found in the cytoplasm. There are several bonding forces involved in the interaction of fGn with the cell membrane, e.g., electrostatic and hydrophobic interactions.[37] The surface hydrophilic groups in fGn improve their adhesion to the hydrophobic lipid bi-layer of cellular structures. It is not only the surface chemistry, but the size of the fGn that influences the cellular uptake mechanism. It is postulated that, due to its smaller size, fGn is taken up by the cell *via* an energy-dependent mechanism. However, it has been shown that, if the fGn nanoparticle is as large as a few μm or a number of graphene sheets are aggregated on top of the membrane, the cellular uptake process most probably occurs through phagocytosis.[3]

Estimating cell viability by measuring mitochondrial dehydrogenase activity

The WST-1 assay is a well-established and widely used assay for detecting and quantifying the cytotoxic effects of xenobiotics by evaluating their effects on the metabolic activity of intact cells by measuring the color change that results from the cleavage of the tetrazolium salt, WST-1, to its formazan form by mitochondrial dehydrogenases.

Cytotoxicity of Gn and fGn—Since fGn was used in the current study primarily as a carrier for delivery of the water-insoluble drug PTL to cancer cells, determination of the cytotoxicity and biocompatibility of these nanomaterials was of obvious interest. The WST-1 assay was used here to compare the cytotoxicity of Gn and fGn in Panc-1 cells after incubation with five concentrations (0–50 μg/ml) of either Gn or fGn (Figure 5). Both forms of graphene showed relatively low cytotoxicity at concentrations <10 μg/ml. When the concentration was increased to 20–50 μg/ml, graphene exhibited higher cytotoxicity than fGn. Graphene has been reported to have milder cytotoxic effects compared to other carbonaceous nanoparticles, such as carbon nanotubes, due to the adsorption of protein corona from the biological medium as a consequence of the large surface area.[38] Overall, in our research, graphene appeared slightly more cytotoxic than fGn at the higher concentrations (i.e., 50 μg/ml); however, 2 way ANOVA (Bonferroni Post-test) analyses of the data determined this difference to be statistically insignificant. Based on these observations, fGn at a concentration of 10 μg/ml was chosen for all the drug treatment experiments described in this study. The hydrophilic nature of the –COOH groups on the

surface of fGn is responsible for the uniform dispersion of fGn in the cell culture medium, creating more contact with the cells without causing high cytotoxicity. Nevertheless, pristine graphene induces a greater cytotoxic effect, as it has a tendency to accumulate on the cellular membrane, producing high levels of oxidative stress at the cellular level, as previously reported in the literature.[39]

Cytotoxicity of PTL, DMAPT, PTL-fGn, and DMAPT-fGn—The IC_{50} values of PTL and its water-soluble analog, DMAPT, in Panc-1 cells were determined in culture using the WST-1 assay and compared to those for PTL-fGn and DMAPT-fGn complexes (Figure 6). The cytotoxic effects of PTL were significantly enhanced by fGn delivery as indicated by the significantly lower IC_{50} value calculated for PTL-fGn (9.5 μM) when compared to that for PTL alone (39 μM). The IC_{50} values for the more water-soluble PTL analog, DMAPT (39 μM), and for DMAPT-fGn (34 μM) indicate that nanodelivery of this compound did not greatly enhance its cytotoxicity. It is possible that the increased cytotoxicity exhibited by the PTL-fGn treatment was the result of higher intracellular concentrations of PTL being delivered to the Panc-1 cells compared to PTL treatment, alone. In the preparation of graphene and PTL-fGn mixtures, there is the possibility of a hydrophobic interaction between PTL and fGn, leading to graphene-mediated active delivery. However, at the same time, the well-dispersed fGn particles are also able to promote enhanced cellular endocytosis and phagocytosis processes,[37] resulting in increased cellular uptake of free drug molecules surrounding the cells, which were otherwise incapable of internalization. PTL, DMAPT and their analogs promote apoptosis by inhibiting the activity of the NF-κB transcription factor complex, indirectly increase reactive oxygen species (ROS), and thereby down-regulate anti-apoptotic genes under NF-κB control[21]. More recently[18], we have shown that PTL and DMAPT analogs also selectively induce almost complete glutathione depletion and cause severe cell death in CD34+ acute myelogenous leukemia cells, but exhibit significantly less toxicity in normal CD34+ bone marrow cells. PTL and DMAPT analogs perturb glutathione homeostasis by a multifactorial mechanism, including inhibition of the key glutathione metabolic enzymes glutamyl-cysteine ligase and glutathione peroxidase, leading to direct depletion of glutathione. In the streptavidin pull-down assay, biotinylated parthenolide interacts with several proteins in AML cells that are all relevant to glutathione function and modulation of ROS. PTL interacts with the following glutathione components of the glutathione pathway: the catalytic unit of glutamyl-cysteine ligase (GCLC), the modulatory unit of glutamyl-cysteine ligase (GCLM), glutathione transferase (GST), glutathione peroxidase (GPX1) and thioredoxin (TXN)[18]. These studies clearly show that, primitive leukemia cells are uniquely sensitive to agents that target glutathione metabolism, resulting in significant increases in ROS and a subsequent increase in lethal double strand DNA breaks.

Quantitation of reactive oxygen species (ROS) levels

Reactive oxygen species (ROS) are chemically reactive molecules containing oxygen. Examples include superoxide radicle, hydroxyl radicle (which results from exposure to ionizing radiation), and peroxide, as well as organic hydroperoxides such as lipid peroxides. ROS are formed as a natural byproduct of the normal metabolism of oxygen and have important roles in cell signaling and homeostasis. However, if ROS levels are allowed to

increase dramatically, this may result in significant damage to cell structures. Cumulatively, this is known as “oxidative stress”. Panc-1 cells were treated with 2',7'-dichlorodihydrofluoresceine diacetate (DCFH-DA) dye to investigate the generation of ROS after 24 hours of treatment with PTL (14 and 30 μM) either delivered alone or by fGn (10 μg/ml; Figure 7). The permeable DCFH-DA dye molecules travel across the cell membrane and are hydrolyzed by cellular esterases to form non-fluorescent 2',7'-dichlorodihydrofluorescein (DCFH), which remains inside the cells. Intracellular ROS oxidize DCFH to form the highly fluorescent 2',7'-dichlorofluorescein (DCF) form. The amount of fluorescent DCF formed is proportional to the intracellular amount of ROS produced. Within 24 hours of incubation, the ROS species in the drug-treated groups significantly increased when compared with cells treated with graphene only ($p<0.001$). Although at the higher concentration (30 μM) there was no significant difference between PTL and PTL-fGn, at the lower concentration (14 μM), PTL-fGn produced a 1.5-fold greater amount of ROS when compared to the same concentration of PTL, alone ($p<0.001$). No increase in ROS concentration was seen when cells were treated with fGn, alone. Maintenance of the intracellular redox system is critical for the survival of a cell. This can be disturbed by enhanced production of intracellular reactive oxygen species (ROS) or a deficiency in the intracellular ROS buffering system, leading to the generation of oxidative stress.[40] Over-production of ROS leads to severe oxidative damage, which includes $\Delta\Psi_m$ depolarization, DNA damage, protein oxidation, and peroxidation of lipids. A number of anticancer drugs induce apoptosis by disrupting the redox system through inactivation of the thiol buffer system and by generation of intracellular ROS.[10] PTL is known to generate ROS by modulating redox homeostasis in several cancer cell lines.[41] These results could indicate that the Panc-1 cells take-up a larger amount of the drug when delivered by fGn, due to improved internalization by endocytosis.

Disruption of mitochondrial membrane potential by PTL and PTL-fGn

Panc-1 cells were treated with JC-1 dye to investigate mitochondrial membrane potential (MMP, $\Delta\Psi_m$) after 24 hours of treatment with PTL (14 μM) either delivered alone or by fGn (10 μg/ml; Figure 8). MMP is indicative of mitochondrial integrity and overall cellular health. Depolarization of mitochondrial membranes or disruption of active mitochondria is an indication of early apoptosis. JC-1 dye is a cationic, lipophilic cell membrane permeable dye that forms a red fluorescent aggregate inside the mitochondrial matrix in healthy cells due to the presence of the inner mitochondrial membrane electrochemical potential gradient. Depolarization of the mitochondrial membrane causes the transition pores to opens preventing accumulation of the dye in the mitochondrial matrix. As a result, the dye is seen as its green (JC-1 monomer) form in the cytoplasm.

Here, untreated cells (negative control) and cells treated with fGn (10 μg/ml), alone, showed almost no sign of MMP dissipation (Figure 8). The Panc-1 cells exposed to 14 μM PTL exhibited comparatively more green fluorescence than the negative control and fGn treatment; however, when the same concentration of PTL was delivered as PTL-fGn, MMP dramatically changed, as evidenced by the bright green fluorescence generated in the few remaining cells. The PTL-mediated ROS generation, like that observed above, has been shown to have a significant effect on mitochondrial health.[13] ROS cause the oxidation of

proteins and lipids that are sensitive to redox oxidation, resulting in mitochondrial damage. The JC-1 staining of these cells indicate that PTL-fGn treatment causes extensive damage to Panc-1 mitochondria. This result is consistent with the WST-1 and ROS detection results and further indicates that nanodelivery by fGn significantly increases the cytotoxicity of PTL.

Detection of Apoptosis after PTL and PTL-fGn treatment

ROS plays a critical role when it comes to signaling in cancer cells. It has been shown that over-production of ROS leads to apoptosis.[42] As a result of excessive ROS production, mitochondrial membranes can be damaged and MMP disrupted. This could then lead to the separation of Bax and Bcl proteins and the eventual release of cytochrome c into the cytoplasm.[43] Once released, cytochrome c can further activate several downstream caspases, which are cystine proteases, and are one of the key factors in apoptosis.[8,44,45] To further investigate and compare the mechanisms of cell death induced by PTL and PTL-fGn treatment, a series of assays to assess cellular apoptosis were carried out.

Caspase activity detection—To provide information on and compare the apoptotic process induced by PTL and PTL-fGn in Panc-1 cells, cell permeable carboxy-fluorescein labeled fluoromethyl ketone (FMK)-peptide caspase inhibitors, which can bind covalently to active caspases (caspase-1, -2, -3, -4, -5, -6, -7, -8, and -9) fluorescently labeling them in situ, were used. The fluorescence of caspase positive cells can be quantified using a fluorescence plate reader (Figure 7b) and visualized using fluorescence microscopy (Figure 8). There was a significant increase in the levels of intracellular caspase measured by the fluorescence plate reader in the PTL-fGn-treated group after just 4 h of incubation ($P<0.05$); although both PTL and PTL-fGn groups showed significant caspase level increases after 14 h, the PTL-fGn treated Panc-1 cells showed a significantly higher level than PTL, alone ($p<0.001$), or than that of the positive control (100 μM of etoposide; $p<0.001$). Once again, this indicates that the cytotoxicity of PTL is significantly enhanced by fGn delivery. The fluorescence microscopy images revealed similar results, as evidenced by the higher levels of green fluorescence, which were generated by most of the PTL-fGn treated cells (Figure 8). The arrows in the inset of the micrograph showing PTL-fGn treatment indicate cellular membrane blebbing and disintegration of the nuclear membrane, the classic morphology of apoptotic cells.

AO/EB staining—AO/EB and DAPI staining were used to visualize and compare the apoptotic process induced by PTL and PTL-fGn treatment (Figure 8). AO is a vital dye and can penetrate cell membranes; EB enters cells only upon membrane disintegration. Healthy, living cells will appear uniformly green. Cells in the early stages of apoptosis will also stain green, but the nuclei will contain bright green spots which are a sign of chromatin condensation and nuclear fragmentation. Late apoptotic cells, which have lost membrane integrity, will also incorporate EB and stain orange. EB/AO staining revealed results similar to those found in the previous experiments. PTL-fGn treated cells showed an increase in apoptotic staining, as evidenced by the red and yellow staining, as well as the low cell numbers.

TUNEL assay—In order to visualize any DNA fragmentation caused by PTL treatment of Panc-1 cells, TUNEL staining was performed (Figure 8). During apoptosis, specific endonucleases are activated, which cause fragmentation or cleavage of genomic DNA in response to apoptotic signals leading to the generation of free 3'-OH groups that can be labeled with terminal deoxynucleotidyl transferase (TdT). The TdT then catalyzes the addition of fluorescein-labeled deoxynucleotides that can be detected by microscopy. Here, the apoptotic nuclei are stained brown by the TUNEL reaction. The PTL-fGn treated Panc-1 cells showed an enhanced amount of nicked DNA after 24 h of incubation as compared with treatment with PTL only. These TUNEL images also support the conclusion that nanodelivery increases the cytotoxicity of PTL in Panc-1 cells.

Flow cytometry analysis after Annexin V &propidium iodide staining—Apoptosis in the Panc-1 cell line after 48 h of PTL and PTL-fGn treatment was measured using flow cytometry analysis of cells stained with Annexin-V and propidium iodide (PI) (Figure 9 and Supplemental Figure 2). Annexin-V detects apoptotic changes in the lipid bilayers and binds to phosphatidyl serine moieties that translocate from the inner membrane to the outer membrane during early apoptosis. PI penetrates and stains cells that have lost membrane integrity. This dual staining method is used to differentiate between apoptotic and necrotic cells. According to the flow cytometry data, after 48 h of incubation with PTL-fGn, 75% of the cells were stained with Annexin-V and/or PI which was higher than the number of stained cells resulting from treatment with PTL, alone (45%). Also, very few cells were found to be only stained with PI, indicating that treatment with PTL causes apoptosis and that nanodelivery of the drug only increases this apoptotic effect. Once more, this supports the conclusion that nanodelivery increases the cytotoxicity of PTL in Panc-1 cells.

Conclusion

The lipophilic sesquiterpene lactone, PTL, has been shown to have promise as an anticancer agent for the treatment of both solid and hematological tumors;[46] however, its poor solubility poses an important challenge to the clinical efficacy and widespread usage of this drug. To solve the problem of poor bioavailability and cellular delivery, we have explored the ability of a carbon-based 2D nanomaterial, fGn, to enhance the cellular uptake and increase the solubility of the drug. We have shown that PTL can be loaded onto fGn nanosheets and that Panc-1 cells exposed to this PTL-fGn complex show increased cytotoxicity as compared to PTL, alone, as indicated by markedly lower IC_{50} values, increased ROS levels, increased MMP disruption, more active caspase, and increased staining by nuclear dyes indicative of apoptosis.

It is postulated that fGn increases the efficacy of PTL by assisting in the drug-internalization process through two different mechanisms: i) fGn provides a highly reactive surface for the drug adsorption based on various chemical interactions, therefore enhancing the water-solubility of the drug and the final complexes; and ii) fGn improves cellular drug uptake into cells, most probably through endocytosis, as carried by the graphene sheets into cells, based on relatively intense electrostatic and hydrophobic interactions.[37] Both of these internalization processes likely produce a significant increase in intracellular drug concentrations, resulting in increased cellular cytotoxicity at reduced drug concentrations.

Therefore, optimization of the chemical surface functionalization of the graphene structures could be the foundation of a technologically tunable approach by which hydrophobic drugs can be solubilized and better delivered to the cells.

The combination of highly active drugs, a nanodelivery platform, could develop into more bio-active nanodrugs, with positive results for the treatment of various cancers. The role of the graphene substrate is rather diverse: it provides a surface for drug decoration, enhances the solubility of the drug, provides a structure for facile and highly sensitive detection *in vitro* and *in vivo*, and establishes a multifunctional platform for drug decoration and the cancer-specific targeting molecules. However, a significant amount of work remains to be done in order to fully understand the toxicity of the graphene itself,[47] its cellular internalization mechanisms,[48] its surface modification when in biologically relevant media due to protein adsorption,[38] and the complex interactions that take place with the subcellular systems.[49, 50]

We have shown that the efficacy of the hydrophobic anticancer drug PTL can be significantly improved *in vitro* using fGn nanomaterials. In addition, many other potent anticancer agents are limited by their lack of water solubility, making their administration difficult and limiting their efficacy. Any improvements in PTL delivery could be extrapolated to improve the efficacy of these other drugs. This approach also has great potential to be expanded to include the addition of targeting molecules to enhance the specific delivery of this compound to cancer cells. Therefore, we expect that the positive effects of fGn drug-delivery presented in this work can be further expanded for complex *in vivo* cancer treatment platforms.

Supplementary Material

Refer to Web version on PubMed Central for supplementary material.

Acknowledgements

Support for this research received from the NIH/National Cancer Institute grant # R01 CA158275 is greatly appreciated. The financial support provided by the US Army TATRC program is also highly appreciated. The editorial assistance of Dr. Marinelle Ringer is acknowledged.

Notes and references

1. Siegel R, Naishadham D, Jemal A. CA: A Cancer Journal for Clinicians. 2013; 63:11–30. [PubMed: 23335087]
2. Safioleas MC, Moulakakis KG. Hepatogastroenterology. 2004; 51:862–868. [PubMed: 15143935]
3. Jang SH, Wientjes MG, Lu D, Au JL. Pharm Res. 2003; 20:1337–1350. [PubMed: 14567626]
4. Li J, Wientjes MG, Au JL. The AAPS Journal. 2010; 12:223–232. [PubMed: 20198462]
5. Von Hoff DD, Ervin T, Arena FP, Chiorean EG, Infante J, Moore M, Seay T, Tjulandin SA, Ma WW, Saleh MN, Harris M, Reni M, Dowden S, Laheru D, Bahary N, Ramanathan RK, Tabernero J, Hidalgo M, Goldstein D, Van Cutsem E, Wei X, Iglesias J, Renschler MF. N Engl J Med. 2013; 369:1691–1703. [PubMed: 24131140]
6. Bork PM, Schmitz ML, Kuhnt M, Escher C, Heinrich M. FEBS Lett. 1997; 402:85–90. [PubMed: 9013864]
7. Pozarowski P, Halicka DH, Darzynkiewicz Z. Cytometry A. 2003; 54:118–124. [PubMed: 12879458]

8. Liu JW, Cai MX, Xin Y, Wu QS, Ma J, Yang P, Xie H-Y, Huang D-S. J Exp Clin Cancer Res. 2010; 29:108. [PubMed: 20698986]
9. Kim JH, Liu L, Lee SO, Kim YT, You KR, Kim DG. Cancer Res. 2005; 65:6312–6320. [PubMed: 16024633]
10. Zhang S, Lin ZN, Yang CF, Shi X, Ong CN, Shen HM. Carcinogenesis. 2004; 25:2191–2199. [PubMed: 15256485]
11. Nakshatri H, Rice SE, Bhat-Nakshatri P. Oncogene. 2004; 23:7330–7344. [PubMed: 15286701]
12. Zhang S, Ong CN, Shen HM HM. Cancer Lett. 2004; 208:143–153. [PubMed: 15142672]
13. Wen J, You KR, Lee SY, Song CH, Kim DG. J Biol Chem. 2002; 277:38954–38964. [PubMed: 12151389]
14. Hehner SP, Hofmann TG, Droge W, Schmitz ML. J Immunol. 1999; 163:5617–5623. [PubMed: 10553091]
15. Wang W, Abbruzzese JL, Evans DB, Chiao PJ. Oncogene. 1999; 18:4554–4563. [PubMed: 10467400]
16. Greten FR, Weber CK, Greten TF, Schneider G, Wagner M, Adler G, Schmid RM. Gastroenterology. 2002; 123:2052–2063. [PubMed: 12454861]
17. Ghosh S, May MJ, Kopp EB. Annu Rev Immunol. 1998; 16:225–260. [PubMed: 9597130]
18. Pei S, Minhajuddin M, Callahan KP, Balys M, Ashton JM, Neering SJ, Lagadinou ED, Corbett C, Ye H, Liesveld JL, O'Dwyer KM, Li Z, Shi L, Greninger P, Settleman J, Benes C, Hagen FK, Munger J, Crooks PA, Becker MW, Jordan CT. J Biol Chem. 2013; 288:33542–33558. [PubMed: 24089526]
19. Guzman ML, Rossi RM, Neelakantan S, Li X, Corbett CA, Hassane DC, Becker MW, Bennett JM, Sullivan E, Lachowicz JL, Vaughan A, Sweeney CJ, Matthews W, Carroll M, Liesveld JL, Crooks PA, Jordan CT. Blood. 2007; 110:4427–4435. [PubMed: 17804695]
20. Shanmugam R, Kusumanchi P, Appaiah H, Cheng L, Crooks P, Neelakantan S, Peat T, Klaunig J, Matthews W, Nakshatri H, Sweeney CJ. Int J Cancer. 2011; 128:2481–2494. [PubMed: 20669221]
21. Shanmugam R, Kusumanchi P, Cheng L L, Crooks P, Neelakantan S, Matthews W, Nakshatri H, Sweeney CJ. Prostate. 2010; 70:1074–1086. [PubMed: 20209491]
22. Nima ZA, Mahmood MW, Karmakar A, Mustafa T, Bourdo S, Xu Y, Biris AS. J BiomedOpt. 2013; 18:55003.
23. Mustafa T, Zhang Y, Watanabe F, Karmakar A, Asar MP, Little R R, Hudson MK, Xu Y, Biris AS. Biomaterials Science. 2013; 1:870–880.
24. Karmakar A, Bratton SM, Dervishi E, Ghosh A, Mahmood M, Xu Y, Saeed LM, Mustafa T, Casciano D, Radominska-Pandya A, Biris AS. Int J Nanomedicine. 2011; 6:1045–1055. [PubMed: 21720516]
25. Xu Y, Karmakar A, Heberlein WE, Mustafa T, Biris AR, Biris AS. Adv Healthc Mater. 2012; 1:493–501. [PubMed: 23184783]
26. Marchesan S, Prato M. ACS Medicinal Chemistry Letters. 2013; 4:147–149. [PubMed: 24900637]
27. Geim AK, Novoselov KS. Nat Mater. 2007; 6:183–191. [PubMed: 17330084]
28. Kopelevich Y, Esquinazi P. Advanced Materials. 2007; 19:4559–4563.
29. Li X, Wang X, Zhang L, Lee S, Dai H. Science. 2008; 319:1229–1232. [PubMed: 18218865]
30. Dikin DA, Stankovich S, Zimney EJ, Piner RD, Dommett GH, Evmenenko G, Nguyen ST, Ruoff RS. Nature. 2007; 448:457–460. [PubMed: 17653188]
31. Stankovich S, Dikin DA, Dommett GH, Kohlhaas KM, Zimney EJ, Stach EA, Piner RD, Nguyen ST, Ruoff RS. Nature. 2006; 442:282–286. [PubMed: 16855586]
32. Li D, Muller MB, Gilje S, Kaner RB, Wallace GG. Nat Nanotechnol. 2008; 3:101–105. [PubMed: 18654470]
33. Qu L, Liu Y, Baek JB, Dai L. ACS Nano. 2010; 4:1321–1326. [PubMed: 20155972]
34. Liu Z, Robinson JT, Sun X, Dai H. Journal of the American Chemical Society. 2008; 130:10876–10877. [PubMed: 18661992]
35. Neelakantan S, Nasim S, Guzman ML, Jordan CT, Crooks PA. Bioorg Med Chem Lett. 2009; 19:4346–4349. [PubMed: 19505822]

36. Vermes I, Haanen C, Steffens-Nakken H, Reutelingsperger C. J Immunol Methods. 1995; 184:39–51. [PubMed: 7622868]
37. Mu Q, Su G, Li L, Gilbertson BO, Yu LH, Zhang Q, Sun Y-P, Yan B. ACS Appl Mater Interfaces. 2012; 4:2259–2266. [PubMed: 22409495]
38. Hu W, Peng C, Lv M, Li X, Zhang Y, Chen N, Fan C, Huang Q. ACS Nano. 2011; 5:3693–3700. [PubMed: 21500856]
39. Sasidharan A, Panchakarla LS, Chandran P, Menon D, Nair S, Rao CN, Koyakutty M. Nanoscale. 2011; 3:2461–2464. [PubMed: 21562671]
40. Buttke TM, Sandstrom PA. Immunol Today. 1994; 15:7–10. [PubMed: 8136014]
41. Khan M, Ding C, Rasul A, Yi F, Li T, Gao H, Gao R, Zhong L, Zhang K, Fang X, Ma T. IntJ Biol Sci. 2012; 8:533–547. [PubMed: 22532787]
42. Afanas'ev I. Aging Dis. 2011; 2:219–230. [PubMed: 22396874]
43. Elmore S. Toxicol Pathol. 2007; 35:495–516. [PubMed: 17562483]
44. Zou H, Li Y, Liu X, Wang X. J Biol Chem. 1999; 274:11549–11556. [PubMed: 10206961]
45. Salvesen GS, Dixit VM. Cell. 1997; 91:443–446. [PubMed: 9390553]
46. Ghantous A, Saikali M, Rau T, Gali-Muhtasib H, Schneider-Stock R, Darwiche N. Cancer Prev Res(Phila). 2012; 5:1298–1309. [PubMed: 23037503]
47. Zhang Y, Ali S, Dervish E, Xu Y, Li Z, Casciano D, Biris AS. ACS Nano. 2010; 4:3181–3186. [PubMed: 20481456]
48. Saeed LM, Mahmood M, Pyrek SJ, Fahmi T, Xu Y, Mustafa T, Nima ZA, Bratton SM, Casciano D, Dervishi E, Radominska-Pandya A, Biris AS. Journal of Applied Toxicology. 2014 In Press.
49. Mahmood M, Villagarcia H, Dervishi E, Mustafa T, Alimohammadi M, Casciano D, Khodakovskaya M, Biris AS. J. Chem. B. 2013; 1:3220–3230.
50. Li Y, Yuan H, vd Bussche A, Creighton M, Furt RH, Kane AB, Gao H. Proceedings of National Academy of Sciences. 2013; 110:12295–12300.

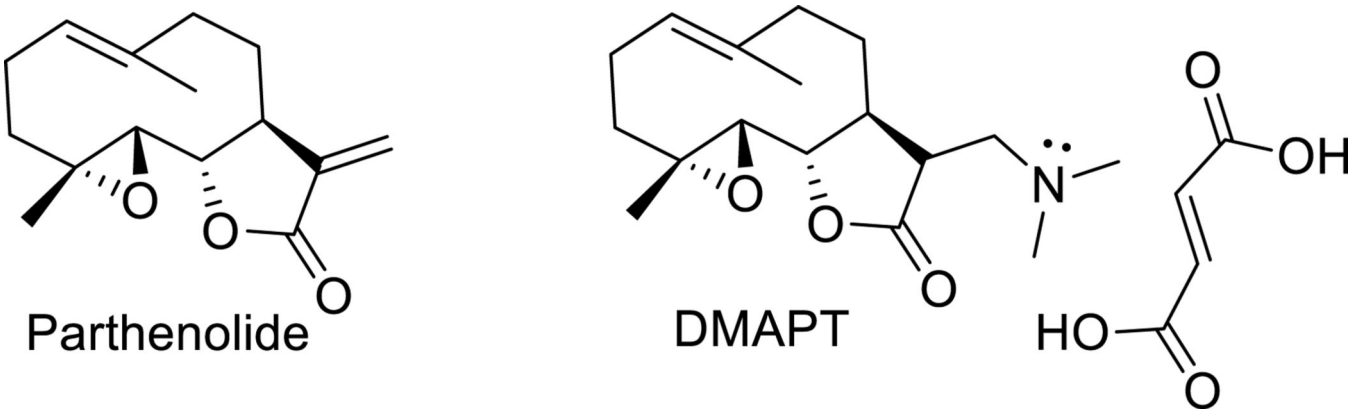

Figure 1.
Structures of Parthenolide and Dimethylamino parthenolide (DMAPT) (as the fumarate salt)

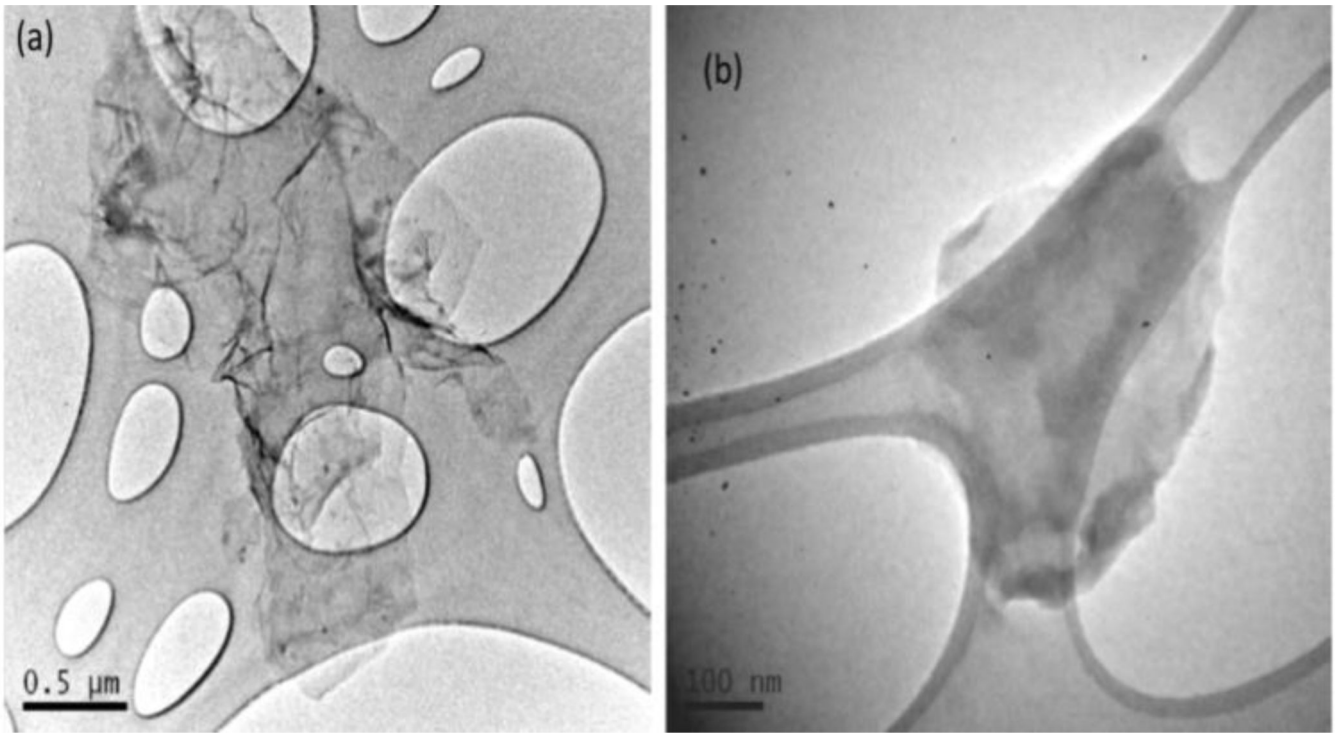

Figure 2.
Transmission Electron Microscopy images of A) Graphene sheet (Gn) and B) functionalized graphene sheet (fGn).

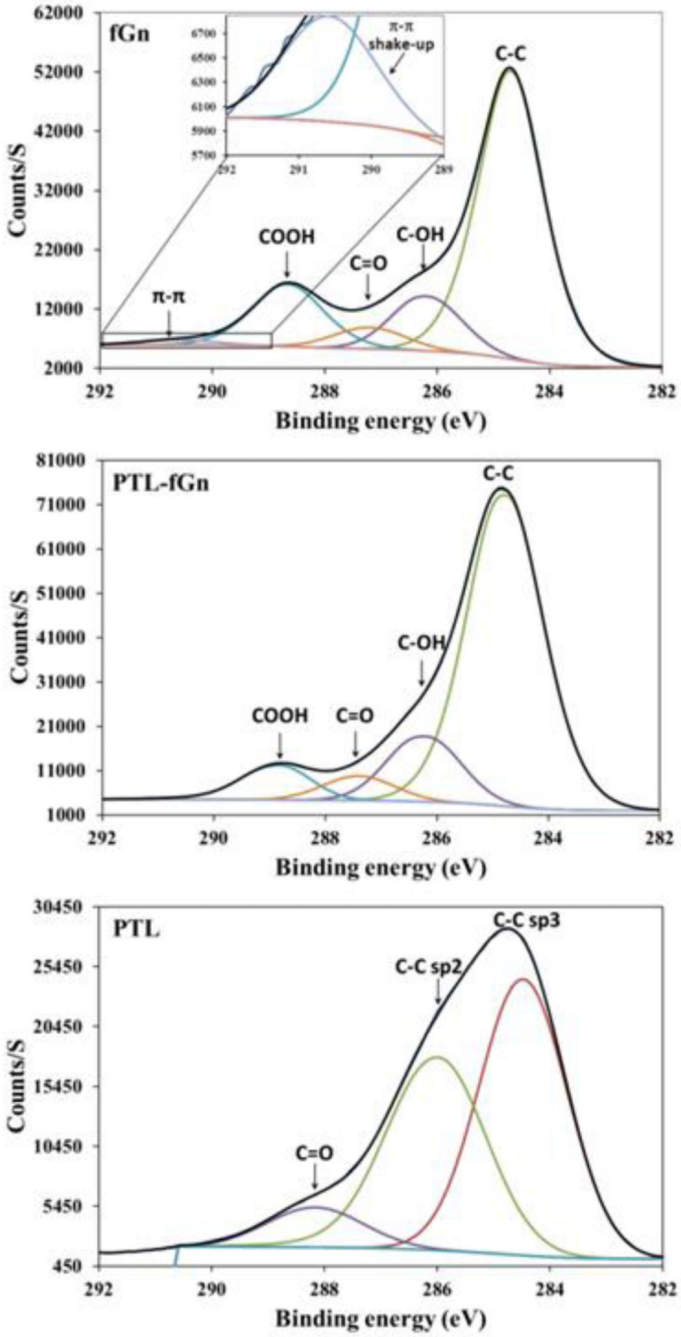

Figure 3.

XPS analysis of fGn, PTL-fGn, and PTL itself. The black traces in each graph represent the C1s signal measured for each material. The peaks below the black traces represent mathematical models of the underlying signals for each moiety (i.e. π-π shake up; C=O, C-OH, COOH, and C-C bonds.) The upper panel contains an inset to show signal representing π-π shake up more detail.

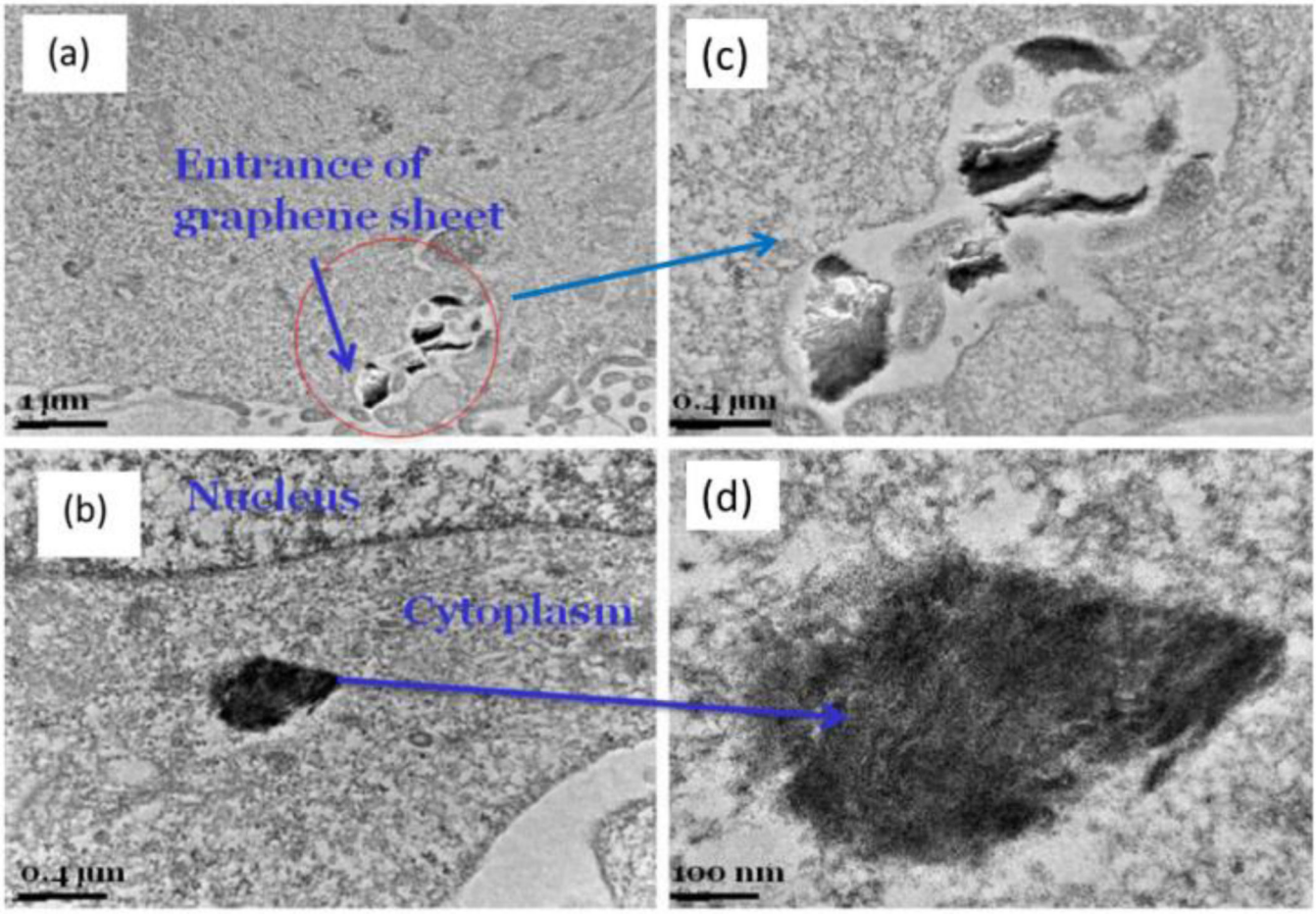

Figure 4.
Low magnification (left column) (a,b) and high magnification (right column) TEM micrographs of fGn internalization by Panc-1 cells (c,d).

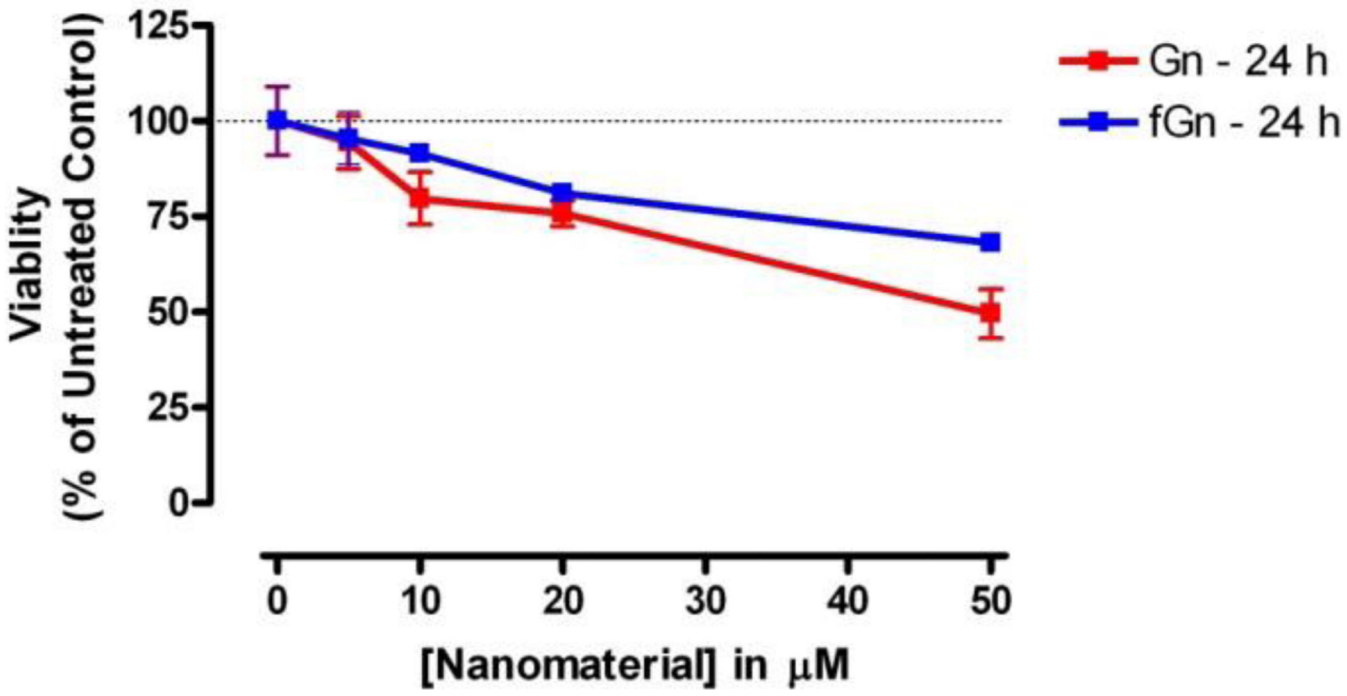

Figure 5.

The concentrations specific cytotoxicity of Gn and fGn. The WST-1 assay was used to determine the cytotoxicity of the carbon nanomaterials on Panc-1 cells. Data represent the mitochondrial dehydrogenase activity of Panc-1 cells after 24 h incubation with increasing concentrations of either Gn or fGn as a percentage of activity in untreated cells.

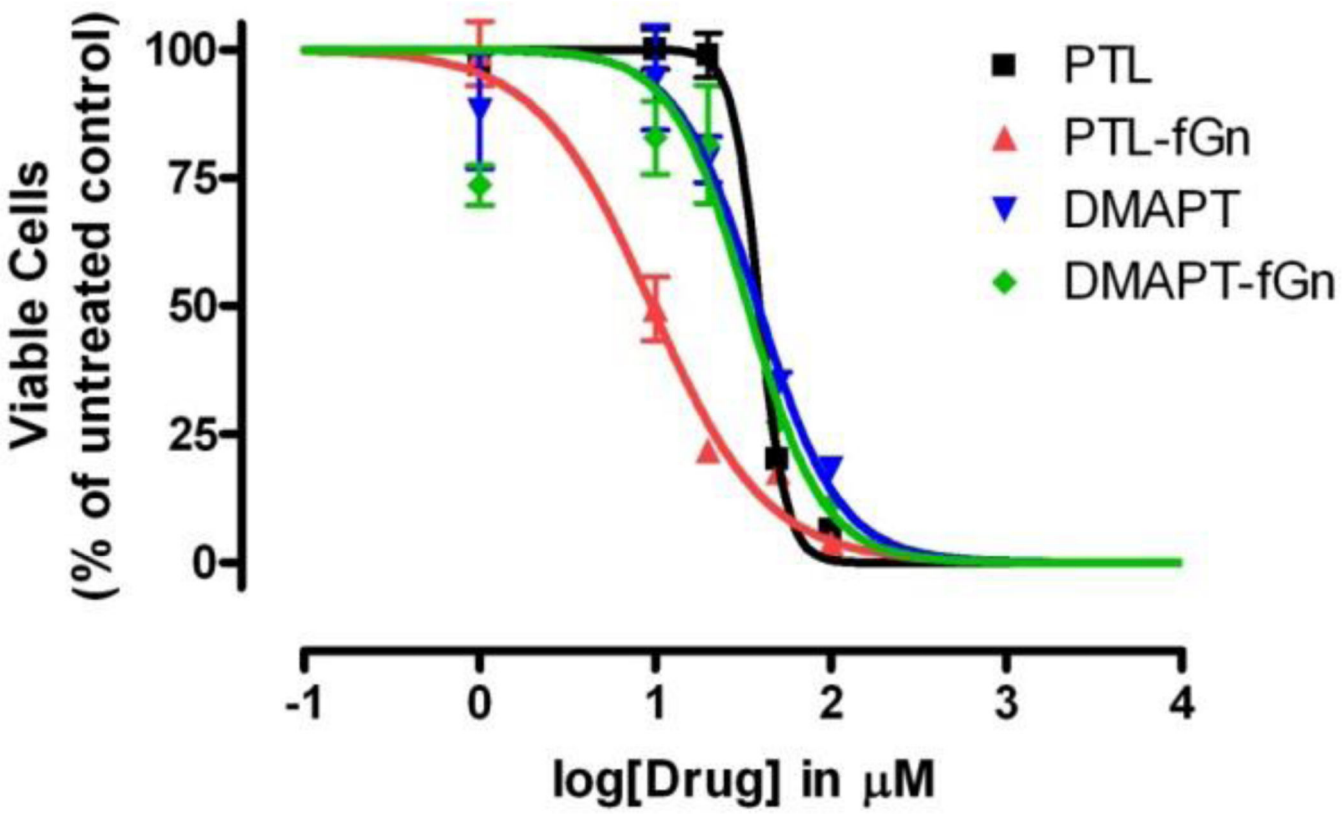

Figure 6.

IC_{50} values for PTL, DMAPT, PTL-fGn and DMAPT-fGn delivered to Panc-1 cells. The concentrations specific cytotoxicity of Gn and fGn was determined by performing the WST-1 assay on Panc-1 cells after 24 h incubations.

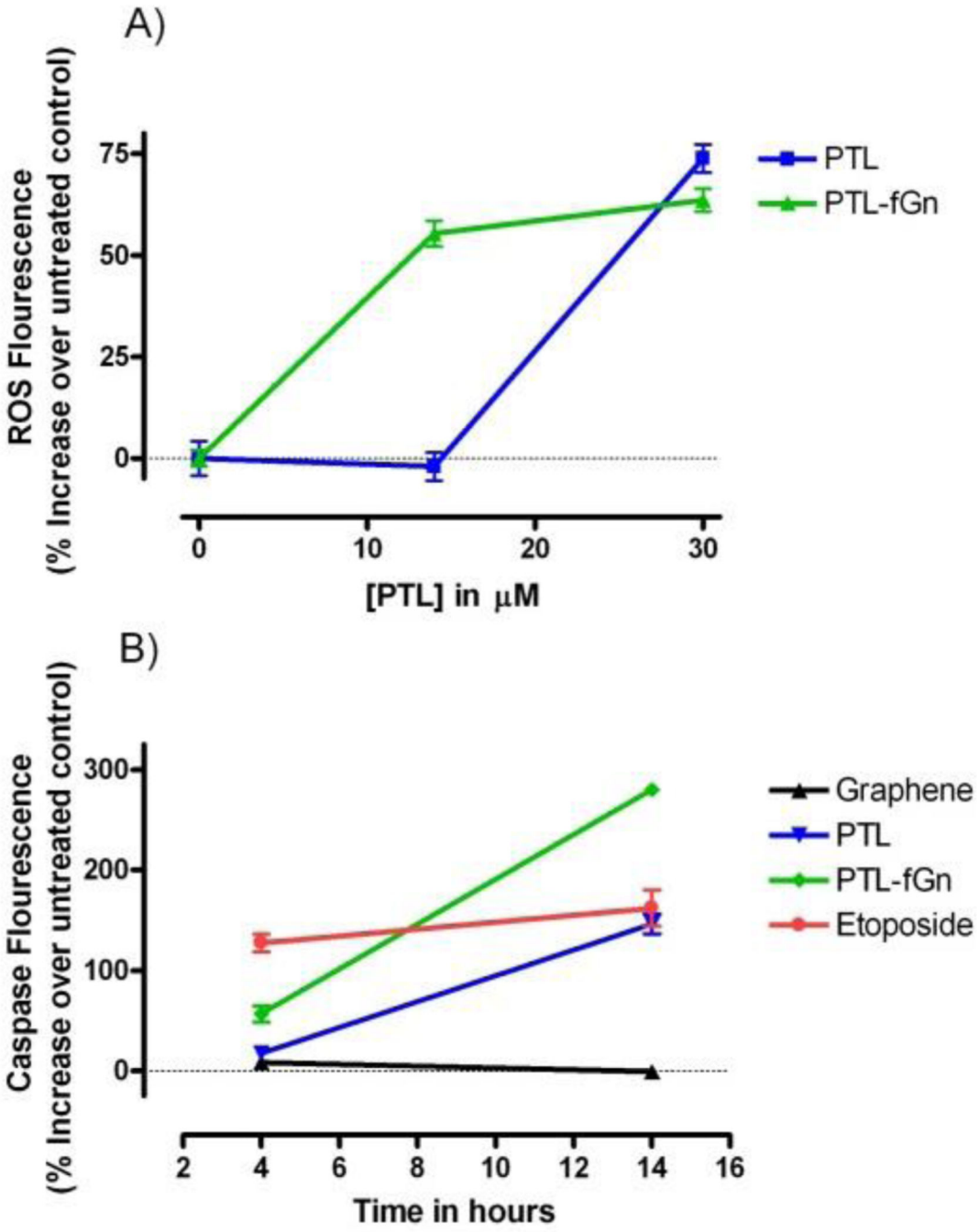

Figure 7.

A) ROS generation. % increases in ROS levels induced by treatment with by PTL and PTL-fGn after 24 hour incubation are shown. No increase was seen when cells were treated with fGn (10 μg/ml) alone. B) Caspase activation. Caspase activity was measured by fluorescence plate reader after 4 and 14 h incubation with PTL and PTL-fGn. Untreated cells and cells treated with only fGn were included as negative controls, and etoposide (100 μM) was included as a positive control.

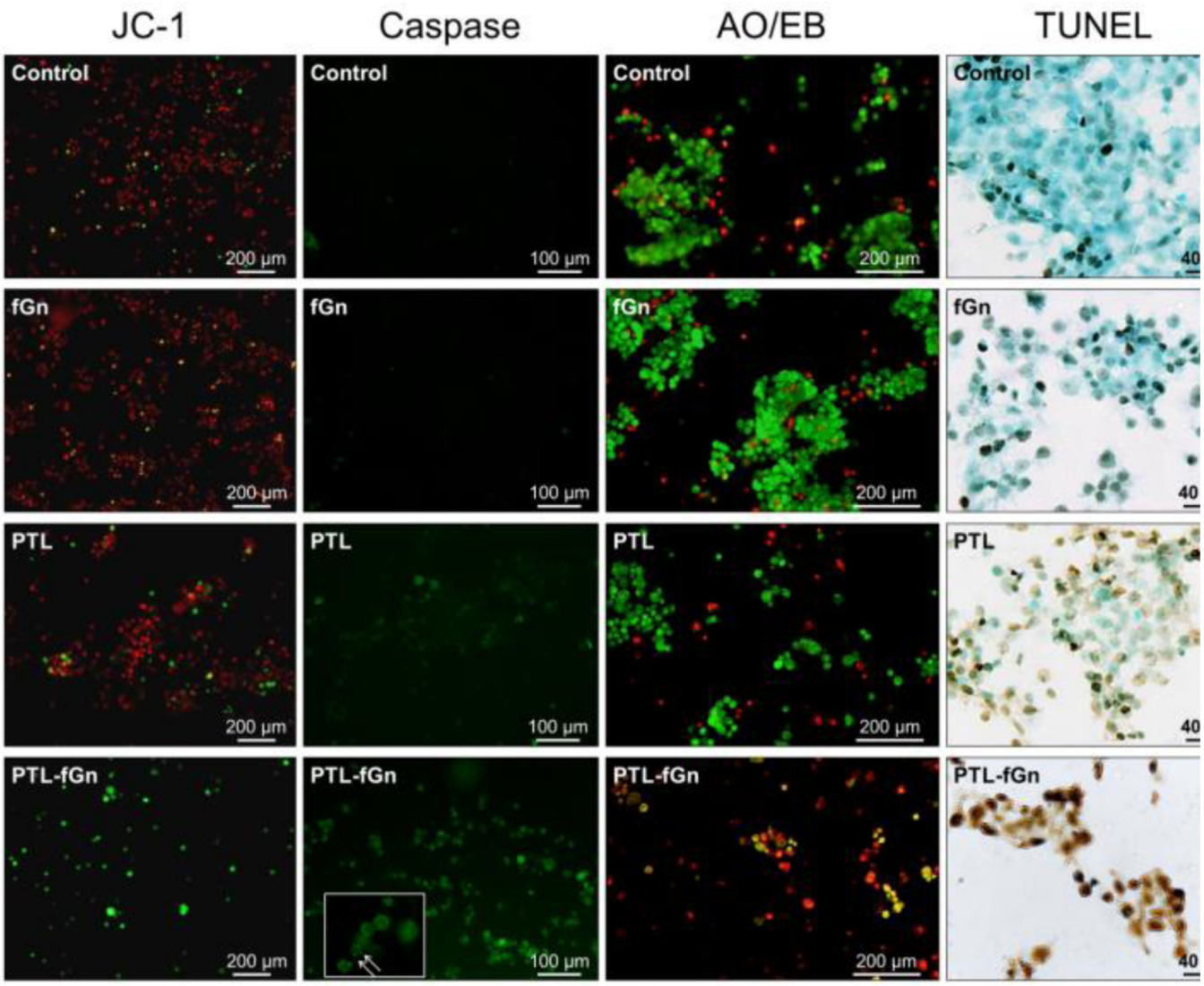

Figure 8.

Microscopy analysis of treated cells stained to detect mitochondrial membrane integrity (JC-1), caspase activity, cell membrane permeability (AO/EB), and DNA fragmentation (TUNEL). Cells were imaged after treatment with PTL and PTL-fGn. Untreated cells and cells treated with only fGn were included as controls. **JC-1**: Red fluorescent JC-1 aggregate forms inside the mitochondrial matrix of cells with healthy mitochondria. Depolarization of the mitochondrial membrane is indicated by the presence of green JC-1 monomer in the cytoplasm. **Caspase**: Healthy cells are unstained (not visible). Cells with active caspases stain green. The inset with arrows shows the apoptotic cells at higher magnification. AO/**EB**: Live cells stain green (AO+), while dead/necrotic cells stain orange (EB+). Cells stained with both dyes will appear yellow. **TUNEL**: Apoptotic nuclei are stained brown by the TUNEL reaction followed by immediate counterstaining of live cells with methyl green.

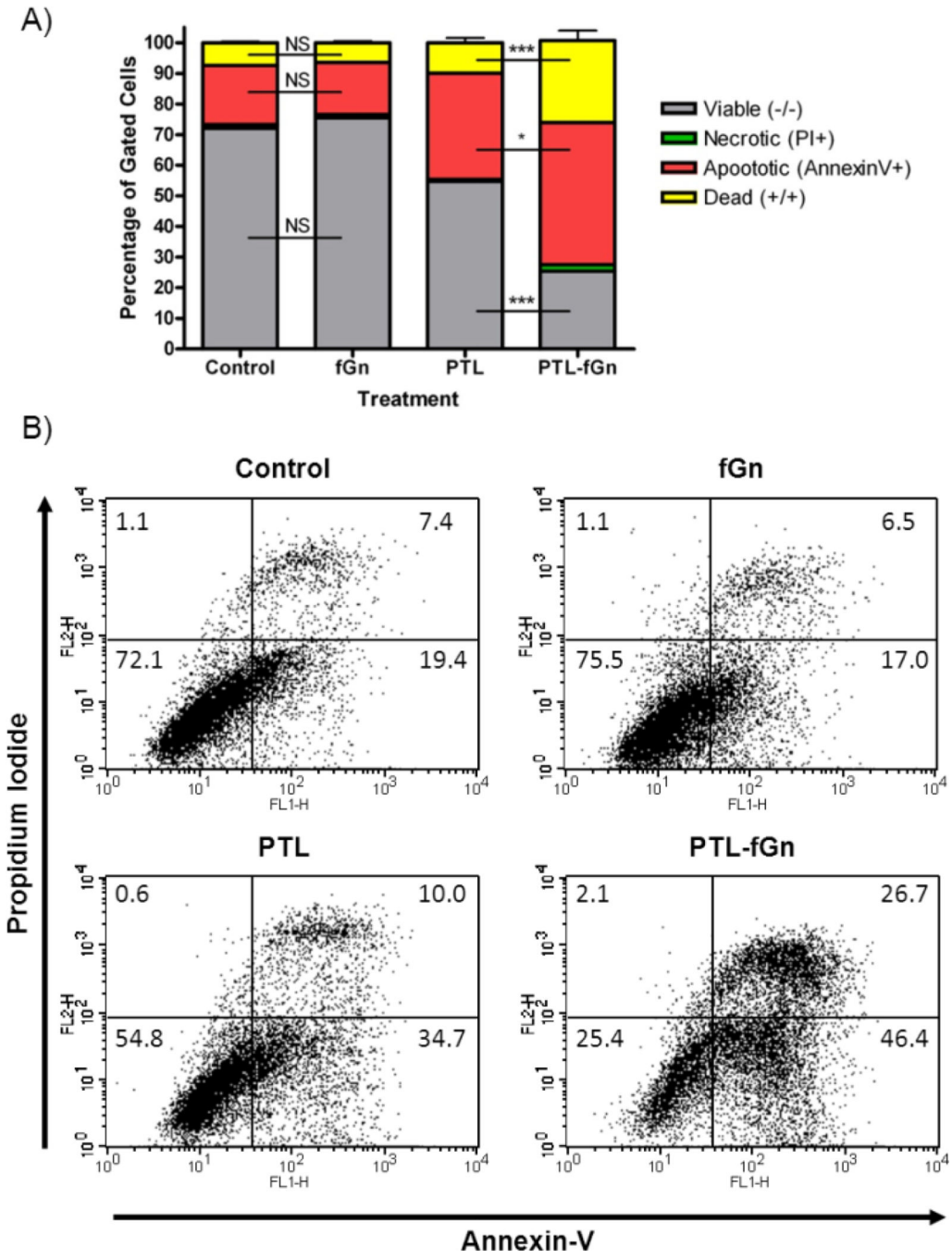

Figure 9.

Flow cytometry analysis of treated cells to detect cell death. data were obtained in cells treated with PTL and PTL-fGn after staining with Annexin-V and PI. Untreated cells and cells treated with only fGn were included as controls. In the flow cytometry plots (B) the lower left corner represents intact, live cells (unstained), the lower right corner represents early apoptotic cells (Annexin-V+), the upper left corner represents the necrotic cells (PI+),

and the upper right corner represents the late apoptotic cells (Annexin-V+; PI+) *=p<0.05; **=p<0.01; ***=p<0.001; NS=Not Significant